LETTER **Communicated by Carson Chow**

Gamma Oscillations in a Nonlinear Regime: A Minimal Model Approach Using Heterogeneous Integrate-and-Fire Networks

Brice Bathellier
brice.bathellier@a3.epfl.ch
Laboratory of Computational Neuroscience and Flavour Perception Group, Brain and Mind Institute, Ecole Polytechnique Fédérale de Lausanne, CH-1015, Lausanne-EPFL, Switzerland

Alan Carleton
alan.carleton@epfl.ch
Flavour Perception Group, Brain and Mind Institute, Ecole Polytechnique Fédérale de Lausanne, CH-1015, Lausanne-EPFL, Switzerland

Wulfram Gerstner
wulfram.gerstner@epfl.ch
Laboratory of Computational Neuroscience, Brain and Mind Institute, Ecole Polytechnique Fédérale de Lausanne, CH-1015, Lausanne-EPFL, Switzerland

Fast oscillations and in particular gamma-band oscillation (20–80 Hz) are commonly observed during brain function and are at the center of several neural processing theories. In many cases, mathematical analysis of fast oscillations in neural networks has been focused on the transition between irregular and oscillatory firing viewed as an instability of the asynchronous activity. But in fact, brain slice experiments as well as detailed simulations of biological neural networks have produced a large corpus of results concerning the properties of fully developed oscillations that are far from this transition point. We propose here a mathematical approach to deal with nonlinear oscillations in a network of heterogeneous or noisy integrate-and-fire neurons connected by strong inhibition. This approach involves limited mathematical complexity and gives a good sense of the oscillation mechanism, making it an interesting tool to understand fast rhythmic activity in simulated or biological neural networks. A surprising result of our approach is that under some conditions, a change of the strength of inhibition only weakly influences the period of the oscillation. This is in contrast to standard theoretical and experimental models of interneuron network gamma oscillations (ING), where frequency tightly depends on inhibition strength, but it is similar to observations made in some in vitro preparations in the hippocampus and the olfactory bulb and in some detailed network models. This result is explained by the phenomenon of suppression that is known to occur

in strongly coupled oscillating inhibitory networks but had not yet been related to the behavior of oscillation frequency.

1 Introduction

Oscillations are a general phenomenon in the brain and develop over a large range of frequencies. However, in awake animals and humans, fast rhythms such as gamma frequencies (20–80 Hz) are especially prominent (Varela, Lachaux, Rodriguez, & Martinerie, 2001). Gamma oscillations are observed during perception in the visual (Singer & Gray, 1995; Gray & Singer, 1989) and olfactory (Wehr & Laurent, 1996; Freeman, 1972; Adrian, 1942) systems, but also during motor control (Schoffelen, Oostenveld, & Fries, 2005) and many other cognitive processes (for review, see Kaiser & Lutzenberger, 2003). This makes them an important correlate of ongoing neural processing and suggests that they might play a determinant role in brain computations (Sejnowski & Paulsen, 2006; Varela et al., 2001). In parallel to phenomenological observations, experimental studies have addressed the question of the mechanisms by which gamma oscillations are generated in brain networks. In particular, pioneering studies could reproduce gamma oscillations in ex vivo preparations, permitting identification, by electrophysiology and pharmacology, of the cellular and synaptic substrates of rhythm generation and control. For the largest part, these experiments were performed in slices of hippocampus (for review, see Bartos, Vida, & Jonas, 2007; Traub, Bibbig, LeBeau, Buhl, & Whittington, 2004), but similar studies were also conducted in preparations of the cortex (Buhl, Tamas, & Fisahn, 1998) and the olfactory bulb (Lagier, Carleton, & Lledo, 2004). In all cases, these experiments demonstrated the involvement of inhibitory circuits, as the oscillation is always disrupted by pharmacological blockade of inhibition. This supports the classic hypothesis that gamma oscillations are resulting from inhibitory feedback loops present in most brain networks (Freeman, 1975). Beyond this important but still schematic idea, several other processes implicated in the oscillation phenomenon were also identified, among them excitatory synaptic transmission, gap junctions, and neuromodulation (Traub et al., 2004). Detailed computational models of realistic spiking neuron networks have attempted to deal with this complexity for the hippocampus (Traub, Whittington, Stanford, & Jefferys, 1996; Bartos et al., 2002) or the olfactory bulb (Davison, Feng, & Brown, 2003; Bathellier, Lagier, Faure, & Lledo, 2006; Lagier et al., 2007). Nevertheless, these models are themselves complex, which together with their specificity prevents the extraction of easily understandable and transposable mechanistic rules.

To this end, analytical methods are better for gaining a physical intuition of the phenomenon and simplifying the search for relevant parameters and physiological mechanisms. An important amount of research has been

conducted in the past 20 years to mathematically formalize spiking neural network oscillations in different regimes and under various assumptions of network architecture, synaptic parameters, and cellular properties. We can, however, categorize the different approaches in two main paradigms. The first (which regroups the larger number of studies) assumes that a population oscillation arises from the phase locking of an ensemble of neurons discharging at a regular and homogeneous frequency, meaning that average network firing rate and oscillation frequency are equal (Strogatz & Mirollo, 1991; Abbott & van Vreeswijk, 1993; Gerstner & van Hemmen, 1993; van Vreeswijk, Abbott, & Ermentrout, 1994; Gerstner, van Hemmen, & Cowan, 1996). In contrast, the second paradigm deals with networks of noise-driven, irregularly firing neurons, whose average firing rate is lower than oscillation frequency. In this case, the population oscillation is in fact imposed by synaptic interactions, which periodically modulate the global firing probability of the network (Brunel & Hakim, 1999; Brunel, 2000; Gerstner, 2000). If both paradigms are applicable to some biological examples, the second one much better fits the irregularity of individual neurons and their relatively low firing rates observed during gamma oscillations in intact animals (Csicsvari, Hirase, Czurko, & Buzsaki, 1998; Friedrich, Habermann, & Laurent, 2004) or in some in vitro preparations (Fisahn et al., 1998; Bathellier et al., 2006). But despite its appeal, this paradigm has been little explored experimentally. A reason for this might be the somewhat indirect approach used to derive these results.

Indeed, the standard analytical approach in this paradigm is to focus on the transition between asynchronous and oscillatory states because this transition occurs via a supercritical Hopf bifurcation (Brunel & Hakim, 1999) for which oscillation behavior can be well captured by a linear analysis. Hence, this approach intrinsically assumes that the amplitude of the firing rate oscillation is small and that its shape is close to a sine function. However, experimental preparations often deal with fully developed oscillations, and, for example, in the case of hippocampal slices, during oscillations the time course of the population firing rate can clearly depart from a sine function and approach a periodic sequence of sharp activity peaks (Fisahn et al., 1998; Hajos et al., 2004). Moreover, while higher-order developments of the linear theory are a possible strategy to deal with the nonlinearities of real oscillations (Brunel & Hakim, 1999), they are limited to the vicinity of the transition point, which is unlikely to cover the parameter range explored in experiments.

To deal with these shortcomings we develop the following theoretical ideas:

- For networks of homogeneous or (or weakly heterogeneous) integrate-and-fire-type neurons, the oscillation period in the limit cycle can be calculated (Gerstner & van Hemmen, 1993; Gerstner et al., 1996; Chow, White, Ritt, & Kopell, 1998; Gerstner, 2000).

- Inhibitory networks receiving heterogeneous but noise-free inputs can generate oscillations in a so-called suppressive regime (Chow, 1998; White, Chow, Ritt, Soto-Trevio, & Kopell, 1998), in which a fraction of the neurons is silenced. This regime can be compared to the low firing rate oscillation of noisy networks in that it yields an average network firing rate smaller than oscillation frequency (if one considers both silent and active neurons).
- Combining the above two ideas, we can compute the full trajectory of the instantaneous network firing rate in the limit cycle. This can be done analytically under some simplifying assumptions (uniform input distribution and current-based synapses; see section 4), while in more realistic cases (gaussian input distribution, partial connectivity, conductance-based synapses; see section 5), the description is reduced to a single iterative equation that is straightforward to solve numerically.
- Because fixed heterogeneities are actually equivalent to slow noise, our results also hold for noise-driven networks under reasonable assumptions on noise correlation time or membrane time constant (see section 6).

In summary, our approach can be seen as a quite general framework to treat oscillations at a low firing rate in a nonlinear regime where the population activity exhibits large periodic activity peaks rather than sinusoidal modulation. The mathematical treatment is based on an intuitive description of the phenomenon. We assume that the oscillation can be decomposed into alternating periods of discharge and complete silence, similar to what is observed in hippocampal in vitro preparations (Hajos et al., 2004) or very commonly in simulations (e.g., see Figure 1). The key to the approach and its novelty is to explicitly model the suppression phenomenon, which decides how many neurons can spike in each cycle and how firing is distributed in time. From the number of spikes per cycle, we can deduce how much inhibition is released after the period of discharge. This feedback inhibition imposes a period of silence, which terminates when inhibition has vanished. Thus, oscillation frequency is finally obtained by computing the time needed for the first neuron to be released from the inhibitory feedback. Because the amplitude of the feedback depends on the period of discharge and reciprocally, computations are performed in a self-consistent manner.

In the end, we obtain a full description of the instantaneous network firing rate, which allows the prediction of the influence of each model parameter and, in particular, the strength of inhibition, which is not straightforward in a traditional framework. We thus can use our mathematical analysis to propose an interpretation of some existing experimental and numerical observations in which network parameters are manipulated. Interestingly, several experiments in the hippocampus and the olfactory bulb showed that varying inhibition strength does not affect oscillation

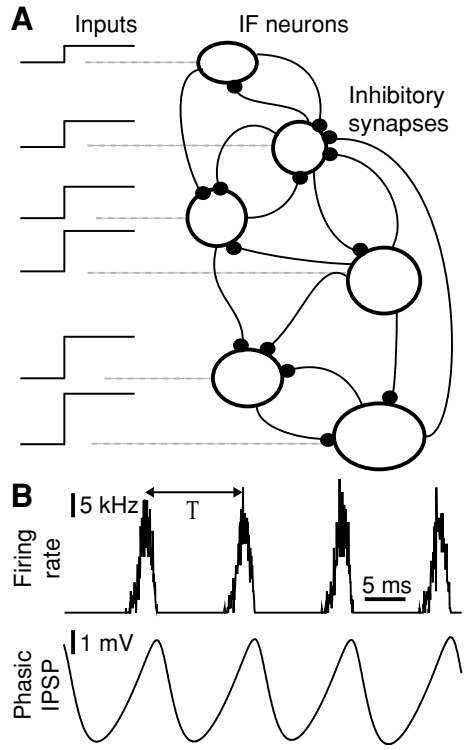

Figure 1: Network and typical ensemble oscillation. (A) Sketch of the network. Neurons receive steady heterogeneous current inputs as well as inhibitory synapses modeled as either currents or conductances. (B) Top: In a typical ensemble oscillation, the firing rate oscillates between periods of discharge and complete silence. Bottom: Subthreshold voltage trace of a single quiescent neuron showing the typical inhibitory phasic inhibitory postsynaptic potential.

frequency, although it can change the network firing rate (Faulkner, Traub, & Whittington, 1998; Fischer & Durr, 2003; Bathellier et al., 2006). This remarkable stability property was also observed in simulations of detailed recurrent inhibitory networks (Kopell & Ermentrout, 2004; Bathellier et al., 2006; Vida, Bartos, & Jonas, 2006) but did not have a clear explanation. In fact, this property cannot be explained according to the standard model of interneuron network gamma oscillation (ING) where all neurons fire on each cycle (Wang & Buzsáki, 1996; Chow et al., 1998; Whittington, Traub, Kopell, Ermentrout, & Buhl, 2000). In this case, the number of spike per cycle is fixed, and the amplitude of the inhibitory feedback that sets the duration of the cycle is proportional to the amplitude of single inhibitory events. In

the suppressive regime that we consider here, inhibition strength controls the amplitude of the inhibitory feedback (and thereby the duration of the silent period) in two antagonist ways: first, via the amplitude of the individual inhibitory events constituting this global feedback, and second, via the number of spikes fired in the period of discharge. We show that while the first one increases with inhibition strength, the second one decreases due to a more rapid suppression of the period of discharge. For sufficiently large heterogeneities (or noise), these two effects tend to be balanced, stabilizing the duration of the oscillatory cycle. This explanation therefore suggests that suppression can play an important role in the mechanism of some gamma oscillations in brain networks.

2 Neural Network Model and Preliminary Assumptions

We consider a network of M leaky integrate-and-fire neurons, each described by its membrane voltage V_i, receiving heterogeneous but constant current inputs I_i^{het} and interconnected by inhibitory synapses (see Figure 1A). When V_i is crossing a threshold θ, the neuron emits a spike, and its voltage is reset to a lower-value V_{reset}. Below threshold, the voltage obeys the differential equation

$$C\frac{dV_i}{dt} = -\frac{1}{R}(V_i - V_L) + I_i^{het} - I_i^{syn}(t), \tag{2.1}$$

where C and R are the membrane capacitance and resistance, respectively, and $I_i^{syn}(t)$ is the total inhibitory current received from synapses.[1] For convenience, we introduce $v_i = V_i - \theta$ and put equation 2.1 in an integral form (starting from the time of the last spike $\hat{t}_i$):

$$v_i(t) = U_i + (V_{reset} - \theta - U_i)e^{-\frac{t-\hat{t}_i}{\tau_m}} - \frac{1}{\tau_m}\int_{\hat{t}_i}^{t} e^{-\frac{t-x}{\tau_m}}\alpha_i(x)\,dx, \tag{2.2}$$

with $\tau_m = RC$, $U_i = V_L - \theta + RI_i^{het}$, and $\alpha_i(t) = RI_i^{syn}(t)$. Note that after this rescaling of voltage, the firing threshold is at $v_i = 0$. A single synaptic input causes a transient current of shape,

$$s(t) = \left(e^{-\frac{t-\tau_l}{\tau_d}} - e^{-\frac{t-\tau_l}{\tau_r}}\right)\Theta(t - \tau_l), \tag{2.3}$$

where τ_d, τ_r, and τ_l are, respectively, the decay time, rise time, and latency of the synaptic event, and $\Theta(t)$ is the Heaviside step function ($\Theta(t) = 1$

[1] Note that here we use current-based synapses; an extension of our approach to conductance-based synapses is discussed in section 5.2

for $t \geq 0$ and zero otherwise). We suppose that the network has all-to-all connectivity,[2] and we describe the activity of the network by a function $\nu(t) = \sum \delta(t - t_i^f)$ where t_i^f is the time of spike f in neuron i. Note that in the limit of large network, $\nu(t)$ is the instantaneous firing rate of the network. The total synaptic current received in a neuron is then

$$\alpha_i(t) = \alpha(t) = J \int_{-\infty}^{+\infty} s(t - x)\nu(x)\, dx, \tag{2.4}$$

where J is the amplitude of a single inhibitory postsynaptic potential. We suppose that the network has reached an oscillatory state, which should typically appear when inhibitory coupling becomes stronger than a critical value J_c (or equivalently, below a critical value of heterogeneity; White et al., 1998; Neltner, Hansel, Mato, & Meunier, 2000; Hansel & Mato, 2003). This oscillatory regime corresponds to a weak locking of neuronal firing for which small time delays are observed between the spikes of different neurons (Gerstner, Ritz, & van Hemmen, 1993; Chow, 1998; Kopell & Ermentrout, 2004). If inhibition is further increased, the oscillation can go in a so-called suppressive regime in which some of the neurons are not able to fire (White et al., 1998; Chow et al., 1998). In addition, this regime typically corresponds to an oscillation in which the network alternates between a period of complete silence and a period of discharge (see Figure 1B). Supposing that we have reached this clearly nonlinear regime and taking T to be the period of an oscillation, we decompose the global firing $\nu(t)$ into a sum of identical T-shifted functions,

$$\nu(t) = \sum_{j=0}^{+\infty} r(t - jT), \tag{2.5}$$

where $r(t)$ represents the time course of the firing during a single oscillation cycle. The hypothesis that the network goes through a true period of silence imposes that $r(t)$ is positive on $[0; T']$ with $T' < T$ and is zero otherwise. In other words, 0 marks the beginning of the period of discharge. Under the assumption of periodic firing, the current received by each neuron (see equation 2.4) can be written in the form

$$\alpha(t) = J \int_{-\infty}^{+\infty} s(t - x)r(x)\, dx + J \sum_{j=1}^{+\infty} \int_{-\infty}^{+\infty} s(t - x)r(x - jT)\, dx, \tag{2.6}$$

which conveniently separates the contribution of synaptic events appearing in the oscillations cycle (i.e., at $t \geq 0$) from those received in previous cycles

[2]Note that an extension of our approach to partial connectivity is discussed in section 5.3.

(i.e., at $t < 0$). The contribution of previous cycles can be computed in two geometrical sums because $s(t)$ is composed of two exponential functions (see equation 2.3). This gives, for $t \in [0; T]$,

$$\alpha_{\text{previous}}(t) = \frac{J\,\mathrm{e}^{-\frac{t+T-\tau_l}{\tau_d}}}{1-\mathrm{e}^{-\frac{T}{\tau_d}}} \int_0^T \mathrm{e}^{\frac{x}{\tau_d}} r(x)\,dx - \frac{J\,\mathrm{e}^{-\frac{t+T-\tau_l}{\tau_r}}}{1-\mathrm{e}^{-\frac{T}{\tau_r}}} \int_0^T \mathrm{e}^{\frac{x}{\tau_r}} r(x)\,dx, \quad (2.7)$$

3 Self-Consistent Equations for the Firing of the Oscillating Network

The integration of synaptic currents in the membrane dynamics (i.e., in equation 2.2) determines when each neuron eventually spikes and thus determines the function $r(t)$. Based on this idea, it is possible to deduce a self-consistent equation for $r(t)$. To do so, we first approximate voltage trajectories for each neuron close to the time of spike emission (i.e., in the period of discharge) and then apply the threshold condition to obtain an equation for spike times.

3.1 Simplification of the Membrane Voltage. We suppose that the population is in an oscillation of (yet unknown) oscillation period T. Each period can be separated in an active phase of duration $T' \leq T$, where many, but not necessarily all, neurons fire, and a silent phase of duration $T - T'$. When integrating the current $\alpha(t)$ in equation 2.2, we make two simplifying assumptions, which are motivated by the nonlinear regime hypothesis and the typical range of neuronal and synaptic parameters in biological networks:

1. We suppose the synaptic rise time τ_r to be small compared to decay time τ_d and to the duration of the silent period $T - T'$ such that $\mathrm{e}^{-\frac{T-T'}{\tau_r}} \ll \mathrm{e}^{-\frac{T-T'}{\tau_d}}$. This is in fact a reasonable assumption for most synapses and for nonlinear oscillations in the gamma range.
2. We suppose that $\mathrm{e}^{-\frac{T-T'}{\tau_m}} \ll \mathrm{e}^{-\frac{T-T'}{\tau_d}}$. On the one hand, the use of this hypothesis is fostered by the observation that oscillations in heterogeneous networks are stable only in the regime where roughly $\tau_m \ll T$ and $\tau_m \ll \tau_d$ (i.e., phasic regime; White et al., 1998).[3] On the other hand, small, effective membrane time constants are typically observed during intense synaptic activity in biological networks due to conductance effects (Destexhe, Rudolph, & Pare, 2003), which

[3]Note that this approximation can very well be valid even if τ_m/τ_d is of the order of few units. For this reason, we keep first-order terms in τ_m/τ_d in the rest of the derivation. This in particular improves numerical agreement with simulations when τ_m/τ_d is rather large, such as in Figures 3 and 4A.

represents another justification of this hypothesis in the extension of our approach to conductance-based synapses.

It follows from the first assumption that during the period of discharge ($t \in [0; T']$), we can neglect the term in τ_r against the term in τ_d in the expression of $\alpha_{\text{previous}}(t)$ in equation 2.7. The second assumption allows us to neglect (i) the influence of the reset that followed the spikes that occurred in previous cycles (see equation 2.2) and (ii) the exponential terms with time constant τ_m that result from the integration of $\alpha_{\text{previous}}(t)$ in the membrane voltage equation (see the last term in equation 2.2). Let us define:

$$N = \int_0^{T'} \mathrm{e}^{\frac{x}{\tau_d}} r(x)\, dx. \tag{3.1}$$

The parameter N represents the number of spikes fired in the period of discharge in each cycle, since we have $x < T' \ll \tau_d$, implying that $\int_0^{T'} \mathrm{e}^{\frac{x}{\tau_d}} r(x)\, dx \approx \int_0^{T'} r(x)\, dx$. Using the previously presented approximations and combining equations 2.2 and 2.6, we obtain an approximate description of the membrane voltage close to the point where a neuron with drive U_i reaches the threshold for the first time after $t = 0$:

$$v_i(t) \simeq U_i - \frac{J\, A_d N \mathrm{e}^{-\frac{t+T-\tau_l}{\tau_d}}}{1 - \mathrm{e}^{-\frac{T}{\tau_d}}} - J \int_0^t v_{\text{single}}(t - x) r(x)\, dx, \tag{3.2}$$

with $A_d = \frac{\tau_d}{\tau_d - \tau_m}$ and $v_{\text{single}}(t)$ being the shape of the membrane voltage variation resulting from a single synaptic event, that is, the convolution of $s(t)$ with the membrane filter ($\mathrm{e}^{-\frac{t}{\tau_m}}$) (here without approximation). This equation is fairly intuitive. The first term on the right-hand side represents the constant drive U_i received by each neuron. The second term describes the fraction of the voltage that results from the synaptic currents received in previous oscillation cycles (i.e, for $t < 0$). It corresponds to the inhibition barrage that prevents firing in the silent period of the cycle (see Figure 2A). The third term describes the fraction of the voltage that results from synaptic currents received during the cycle (i.e., for $t \geq 0$) from neurons that have spiked just before neuron i. Contrary to the second term, this term tends to increase over time during the period of discharge (i.e., accumulation of new synaptic events; see Figure 2B). By progressively bringing neurons away from threshold, this term actually mediates the suppression phenomenon and terminates activity during each cycle.

3.2 Equations for the Oscillation Period and Single Neuron Spike Times. We now suppose that each neuron of the network fires at most once in a cycle as it is commonly observed in brain slice experiments (Fisahn et al., 1998; Bathellier et al., 2006). This allows us to deduce all spike times

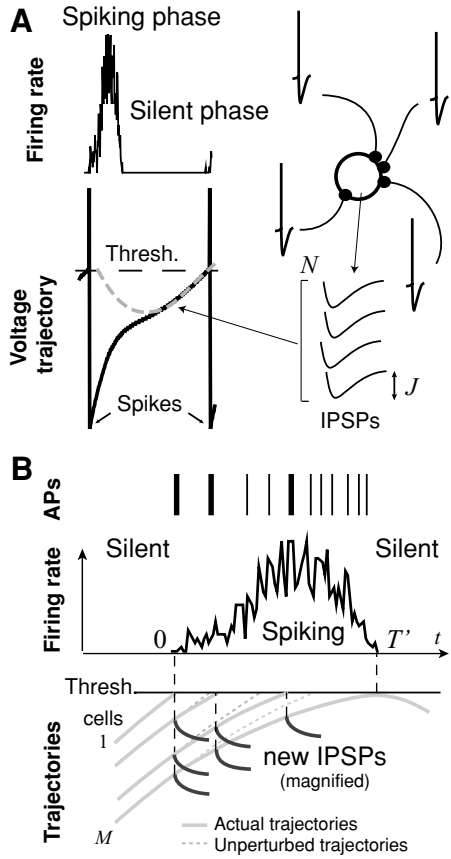

Figure 2: Mechanisms of the oscillation. (A) The silent period is imposed by the barrage of inhibitory events (IPSPs) generated during the period of discharge. The duration of the silent period depends mainly on waveform of the global IPSP (gray dashed line superimposed onto the voltage trace). (B) The spiking phase resumes when the first neuron reaches threshold—first action potential, (AP) in the AP sequence. The voltage trajectories in subsequent neurons are deviated downward by the new IPSPs coming from preceding neurons (compare actual trajectories with trajectories in the absence of IPSPs, i.e., unperturbed). Ultimately these IPSPs suppress the spiking of the less excited neurons, leading to the end of the period of discharge.

directly from equation 3.2 and forget about the dynamics of neurons right after reset (except that we assume the reset to be strong enough to prevent any neuron from firing again before the end of the period of discharge). Spike time t_i in each neuron i is given by the threshold condition $v(t_i) = 0$. However, the period of discharge starts by definition at time $t = 0$, when

inhibition has vanished enough for a first neuron (denoted i_0) to reach the firing threshold (see Figure 2B). At this time point, applying $v_{i_0}(0) = 0$ to equation 3.2 gives an equation for the oscillation period:

$$U_{i_0} = \frac{J N A_d \mathrm{e}^{-\frac{T-\tau_l}{\tau_d}}}{1 - \mathrm{e}^{-\frac{T}{\tau_d}}}. \tag{3.3}$$

In fact, because all neurons are supposed to receive the same synaptic currents here, the first neuron to fire is the one with the largest current drive, so $U_{i_0} = \max(U_i,\ i \in [1 : M])$. The threshold is then reached by other neurons, following the inverse order of their current drives (see Figure 2B). Therefore, we order the neurons decrementally according to their current input with index k. We also now take $r(t) = \sum \delta(t - t_k)$, where t_k represents the time of the spike in neuron k. By combining equations 3.2 and 3.3, we obtain an equation for the time of each spike in the oscillation cycle:

$$U_k = U_{i_0} \mathrm{e}^{-\frac{t_k}{\tau_d}} + J \sum_{i=0}^{k-1} v_{\text{single}}(t_k - t_i). \tag{3.4}$$

Because we know the distribution of the U_k, this equation can be solved by recurrence until a value K (note that $K \approx N$) for which a jump in the solution is observed ($t_K - t_{K-1} \gg t_{K-1} - t_{K-2}$). This marks the end of the period of discharge ($T' = t_{K-1}$) and occurs when the second term on the right-hand side has increased enough (i.e., the newly generated inhibitory currents are able to silence neurons with the weakest drives; see Figure 2B). Having the t_k's and thereby the quantity N, it is straightforward to compute the period T via equation 3.3, leading to a full description of the oscillation. It noteworthy that T here explicitly depends on the product $J N$ (amplitude of a single inhibitory event times roughly the number of spikes fired in a cycle), but that N will decrease with an increasing J via the feedback process appearing on the left-hand side of equation 3.4 and which drives the suppression of firing. Therefore, the description obtained here fairly well summarizes the intuitive argument made in section 1 to explain the stability of the oscillation period with respect to J. But the exact dependencies of N in J and other parameters are still unknown. They can, however, be explored by solving the spike time equation (see equation 3.4).

4 Analytical Solution of the Spike Time Equation for a Uniform Heterogeneity Distribution

Explicit solutions of the spike time equation are difficult to obtain in the general case. But if we suppose that the distribution of heterogeneities is uniform and the number of neurons is large, it is possible to derive a continuum

equation, which can be solved analytically. While such a distribution is not commonly observed in most biological networks, the analytical results obtained in this section are still mostly valid to explain the qualitative behavior of more realistic models, as we show in section 5.

4.1 Derivation and Resolution of the Continuum Equation. The continuum equation is obtained in the limit of large networks ($M \to \infty$) for which $r(t)$ becomes the instantaneous firing rate of the network and the interspike intervals go to zero ($t_{k+1} - t_k \to 0$). Continuous and discrete descriptions can be linked by the relation $\int_{t_k}^{t_{k+1}} r(x)\,dx = 1$, which becomes $(t_{k+1} - t_k)r(t_k) = 1$ when approximated to the first order in $t_{k+1} - t_k$. When a first-order development of equation 3.3 is used for two consecutive spikes, the interspike interval can also be expressed as

$$U_{k+1} - U_k = (t_{k+1} - t_k)\frac{\mathrm{d}}{\mathrm{d}t}\left(U_{i_0}\mathrm{e}^{-\frac{t}{\tau_d}} + J\int_0^t r(x)v_{\mathrm{single}}(t-x)\,dx\right)_{t_k}. \quad (4.1)$$

The combination of these two expressions for the interspike interval gives an equation for $r(t)$, provided that we can approximate the random uniform distribution of input drives by a regular distribution $U_k = U_{\max} - k\frac{\Delta U}{M}$ where $\Delta U = U_{\max} - U_{\min}$ is the width of the distribution and M the total number of neurons:

$$r(t) = -\frac{M}{\Delta U}\frac{\mathrm{d}}{\mathrm{d}t}\left(U_{i_0}\mathrm{e}^{-\frac{t}{\tau_d}} + J\int_0^t r(x)v_{\mathrm{single}}(t-x)\,dx\right). \quad (4.2)$$

If we take $\tau_l = 0$ (i.e., no latency) and exploit that the integral represents a convolution by three exponential terms, equation 4.2 becomes an inhomogeneous third-order linear differential equation. However, to reduce the complexity of the solution, we assume that $T' \ll \tau_d$, which is typically observed in the nonlinear regime (e.g., see Figures 1 and 3), and we obtain a second-order differential equation (the derivation is detailed in appendix A),

$$\tau_m\tau_r\frac{\mathrm{d}^2 r}{\mathrm{d}t^2} + (\tau_m + \tau_r)\frac{\mathrm{d}r}{\mathrm{d}t} + \left(1 + \frac{JM}{\Delta U}\right)r(t) = \frac{MU_{i_0}}{\tau_d\Delta U}, \quad (4.3)$$

with initial conditions $r(0) = \frac{M}{\tau_d}\frac{U_{i_0}}{\Delta U}$ and $\frac{\mathrm{d}r}{\mathrm{d}t}(0) = 0$.

For the solution of this equation to cross zero at least once for positive times (which is required to fulfill the hypothesis that network discharge in a cycle spans a finite time interval), it is necessary that the quantity $\delta = 4\frac{\tau_m\tau_r(1+JM/\Delta U)}{(\tau_m+\tau_r)^2} - 1$ be positive (this condition can be seen as a rough approximation of the minimal inhibition strength at which a stable or unstable oscillatory solution for the network firing rate exists). In this case, setting

$a = \frac{1}{2\tau_m} + \frac{1}{2\tau_r}$ and $b = a\sqrt{\delta}$, we obtain the time course $r(t)$ of the firing rate in each cycle:

$$r(t) = \frac{U_{i_0}}{\tau_d J} \frac{\frac{JM}{\Delta U}}{1 + \frac{JM}{\Delta U}} \left(1 + \frac{JM}{\Delta U}\left(\cos(bt) + \frac{1}{\sqrt{\delta}}\sin(bt)\right)e^{-at}\right). \tag{4.4}$$

In the limit of $T' \ll \tau_d$, equation 3.3 for the period of the oscillation can be rewritten as

$$T = \tau_d \ln\left(\frac{JA_d}{U_{i_0}} \int_0^{T'} r(x)\,dx + 1\right), \tag{4.5}$$

where T' is the time at which network activity terminates (i.e., the solution of $r(T') = 0$). These solutions are observed to be in rather good agreement with simulations of the full network, especially for oscillations that are far from the transition between the asynchronous and oscillatory state (see Figure 3). They are also very close to the numerical resolution of equations 3.4 and 3.3 (see Figure 3). Unsurprisingly, the quality of frequency predictions decreases close to the bifurcation (see Figure 3B). This is due to the terms neglected when deriving equation 3.2, in particular, the voltage reset following spikes. The latter term tends to make neurons fire later in a cycle (or be suppressed) than when they are fired in the previous one (this in fact explains that the firing period is slightly longer in simulations, e.g., Figure 3A). We observed that this results in either the destabilization of the oscillation or the creation of additional slower frequencies in some conditions (in some cases, a small proportion of neurons can be observed to fire in a fraction of the cycles). But interestingly, we find in any case, an excellent agreement between analytical results and simulations for the time-averaged network firing rate $\nu_0 = 1/T \int_0^T r(t)dt$, after but also before the bifurcation (see Figure 3B).

4.2 Solution and Parameter Dependencies in the Limit of Strong Inhibition. Because the nonlinear regime is typically obtained for large amplitudes of inhibition, it is interesting to consider the limit $JM \gg \Delta U$. In this case, formula 4.4 can be simplified into

$$r(t) = \frac{U_{i_0}}{\tau_d J} \frac{JM}{\Delta U} \cos(\tilde{b}t)e^{-at}, \tag{4.6}$$

where $\tilde{b} = \frac{2a}{\tau_m + \tau_r}\sqrt{\frac{JM\tau_m\tau_r}{\Delta U}}$. The duration of the discharge becomes $T' = \pi\tilde{b}^{-1}$. Using the fact that for $JM/\Delta U \gg 1$, we have $1/T' \sim \tilde{b} \gg a$, we also obtain

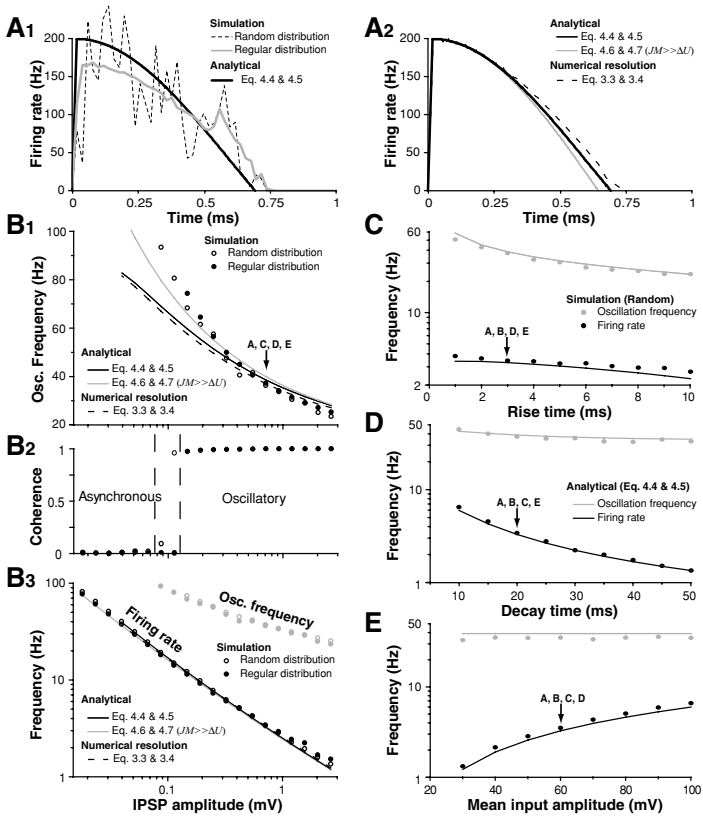

Figure 3: Oscillation in a network receiving a uniform distribution of inputs and all-to-all connectivity. (A) Firing rate during the spiking period in simulations for a random and a regularly interspaced distribution of inputs (mean of 40 periods) and predictions of our theoretical framework (analytical and numerical solutions of the spike time equation are shown). (B) Oscillation frequency (B1), coherence (B2), and network average firing rate (B3) when inhibition strength is varied: simulations and theoretical predictions. In *B1*, no finite solutions of equation 4.4 or equation 3.3 are found found beyond the left end of the curves. Coherence is the mean vector strength ($\sqrt{\langle \sin \phi_i \rangle^2 + \langle \cos \phi_i \rangle^2}$) of the spike phases ($\phi_i$) measured between successive peaks of the membrane voltage averaged over the entire population. The dashed line in *B2* indicates the transition between asynchronous and oscillatory states observed in simulations. (C–E) Simulations and theoretical predictions of oscillation frequency and mean firing rate for variations of the synaptic rise (C) and decay (D) time, and of the mean input current while ΔU is kept constant (E). Simulation parameters when not varied: $M = 961$ neurons, $\theta = -52$ mV, $V_{\text{reset}} = V_L = -70$ mV, $\tau_m = 5$ ms, $U = \langle U_i \rangle = 60$ mV, $\Delta U = 0.2 \langle U_i \rangle$, $\tau_d = 20$ ms, $\tau_r = 3$ ms, $\tau_l = 0$. In *A, E, F*, and *G*, $J = 0.71$ mV.

from the integration of $r(t)$ in equation 4.5 a simple closed-form formula for the period of oscillation:

$$T = \tau_d \ln\left(\sqrt{\frac{J\,M}{\Delta U}}\frac{\sqrt{\tau_r\,\tau_m}}{\tau_d - \tau_m} + 1\right), \tag{4.7}$$

which is in fact numerically similar to the nonsimplified solution (see equations 4.4 and 4.5) far from the bifurcation (see Figure 3B). This expression clearly shows that the important parameters for the determination of oscillation frequency are synaptic and membrane time constants as well as the ratio of inhibition over network heterogeneities (i.e., the dispersion of membrane voltages ΔU).

The dependency on τ_m and τ_r can be understood intuitively. Both parameters are setting the rise of inhibitory events, which controls the number of spikes fired in each cycle. Slower rise of inhibition implies slower silencing and thus more spikes. This strengthens the global inhibitory feedback that follows the discharge and prolongs the period of silence, thereby decreasing oscillation frequency (see Figure 3C). The same intuitive explanation could be given for the role of inhibition latency, although it was not considered here in the analysis (but see Figure 5A).

The role of the decay time τ_d is less intuitive. Because it controls the duration of inhibitory events, τ_d sets the duration of the period of silence. But it also determines the rate at which neurons of the population cross the threshold during the period of discharge (via the slope of the membrane potential; see equation 3.4). Therefore, it also controls the number of spikes fired in the cycle (which is represented by the term inside the logarithm in formula 4.7). For large τ_d, these effects tend to compensate for each other, canceling the influence of τ_d on population frequency (see Figure 3D). Interestingly, the influences of τ_d and τ_r on frequency, observed here in a heterogeneous network, are similar in noisy networks (Brunel & Wang, 2003).

It is also noteworthy that while the spread ΔU of heterogeneities contributes in setting the oscillation frequency, the average drive $\langle U_i \rangle$ does not have any influence (see Figure 3E). However, the time-averaged network firing rate depends linearly on this parameter.

Finally, the dependency on inhibition strength is weak (i.e., via the logarithm of a square root; see also Figure 3B), which corresponds to observations made in simulations of comparable heterogeneous networks (Kopell & Ermentrout, 2004). This weak dependency is explained by the fact that the decrease in the number of spikes per cycle for larger inhibition does not perfectly balance the increase of the strength of individual synaptic current. As a result, the period of silence becomes longer, and frequency decreases. Importantly, formula 4.7 clearly shows that oscillation frequency cannot reach an extremum (or a plateau) for large J as observed in some

numerical studies of more realistic networks (Bathellier et al., 2006; Vida et al., 2006) and in some experiments (Bathellier et al., 2006; Fischer & Durr, 2003; Faulkner et al., 1998). In order to obtain this behavior, it is necessary to extend the model to more realistic assumptions, as we show in the next section.

5 Extensions to Biologically Realistic Neuronal and Network Features

5.1 Gaussian Distributions of Heterogeneities. For any distribution of inputs, it is straightforward to solve equation 3.4 numerically, supposing, for generality, that inputs are distributed regularly (i.e., $U_k = F^{-1}(1 - k/M)$ where F is the cumulative distribution function and M the total number of neurons). We can therefore also easily predict both the firing rate and oscillation frequency for a gaussian distribution of inputs, which are more likely to approximate the reality of biological neural networks. This prediction rather well approximates simulations of the full network (e.g., see Figure 4A). The main discrepancy between uniform and gaussian distributions is that for the latter, the voltage difference between two consecutive neurons ($\Delta U/M$ in the uniform distribution) is larger in the tails than in the center of the distribution, meaning that the level of heterogeneity is locally higher. For example, this attenuates the decrease of frequency for strong inhibition that progressively restricts the firing to neurons in the upper tail of the distribution and increases heterogeneities (see Figure 4A; see also the effect of increasing ΔU in equation 4.7). This effect is, however, not strong enough to yield a minimum or a plateau of frequency for large J. It is noteworthy that this effect is also responsible for a decrease of frequency when the mean of the input distribution is increased while the variance is kept constant (e.g., see Figure 5D), which is not observed for the uniform distribution (see Figure 3E).

5.2 Conductance-Based Synapses. In real neurons, synaptic currents are the result of conductance changes and therefore depend on membrane voltage. If we account for this property in our model, the total synaptic current has to be written as $I_i^{syn}(t) = (V(t) - E_{syn})G_i(t)$, where E_{syn} is the reverse potential of the synapses and $G_i(t)$ is the total synaptic conductance. However, under the assumptions that $G(t)$ varies little around its average and that the membrane voltage stays close to threshold (see appendix B), the conductance-based model can be reduced to a canonical voltage equation similar to the one introduced for the current-based model (see equation 2.2). The only difference with the latter is that we have to work with an effective membrane time constant $\tau_m^* = \frac{RC}{1+R\langle G\rangle_t}$, which depends on the time average of the total inhibitory conductance $\langle G\rangle_t$. Supposing that a single synaptic opening leads to a maximum conductance $G_{\max}$ with a transient time course

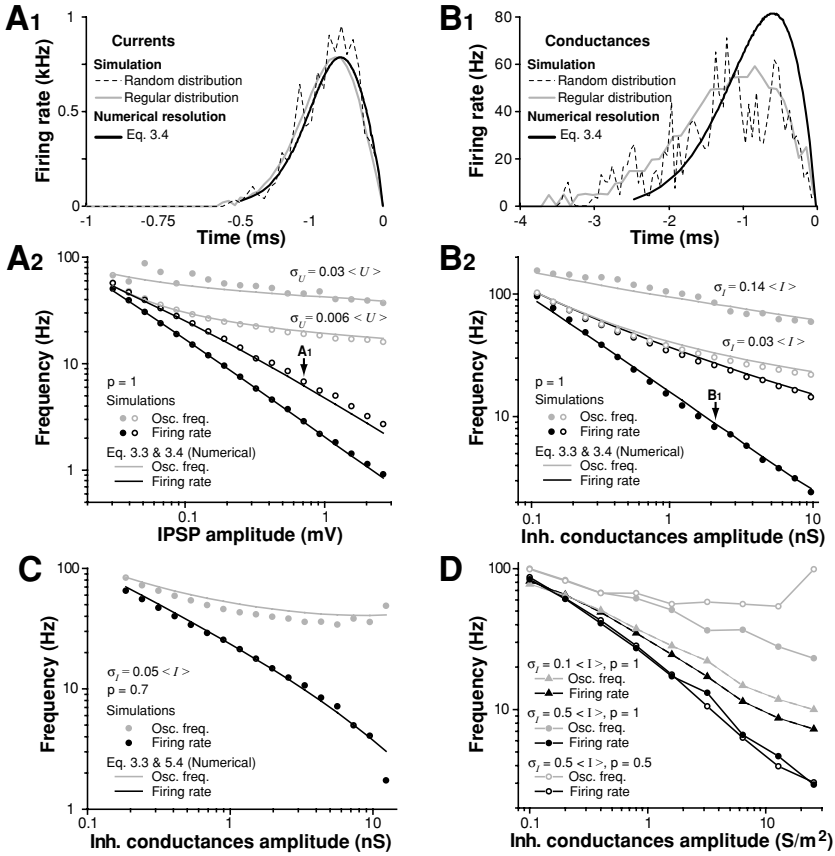

Figure 4: Oscillation robustness to changes in inhibition strength. (A) Network with a gaussian distribution of inputs and synapses modeled as currents. (A1) Instantaneous population firing rate during the period of discharge in simulations compared to numerical results based on our theoretical framework (solution of equation 3.4). $\sigma_U = 0.006\ \langle U \rangle$ and $J = 0.71$ mV. (A2) Oscillation frequency and firing rate in simulations compared to our theoretical predictions for two different values of input variance $\sigma_U = R\sigma_I$. All parameters except σ_U are the same as in Figure 3. (B) Same as A but with synapses modeled as conductances. Parameters: $M = 961$ neurons, $R = 100$ MΩ, $C = 500$ pF, $\theta = -52$ mV, $V_{\text{reset}} = \text{VL} = -70$ mV, $VG = -70$ mV, $\langle I \rangle = 3$ nA, $\tau_d = 10$ ms, $\tau_r = 2$ ms, $\tau_l = 1$ ms. In $B1$, we took $\sigma_I = 0.14\langle I \rangle$ and $J = 2$ nS. (C) Same as $B2$ but for random connectivity and connection probability $p = 0.7$. Note that oscillation frequency goes through a minimum when inhibition strength is large. Parameters are the same as in B. (D) Simulations of a network of 100 detailed neurons taken from (Bathellier et al., 2006), for all-to-all (filled symbols) and partial connectivity (empty circles). A minimum in oscillation frequency is observed for partial connectivity.

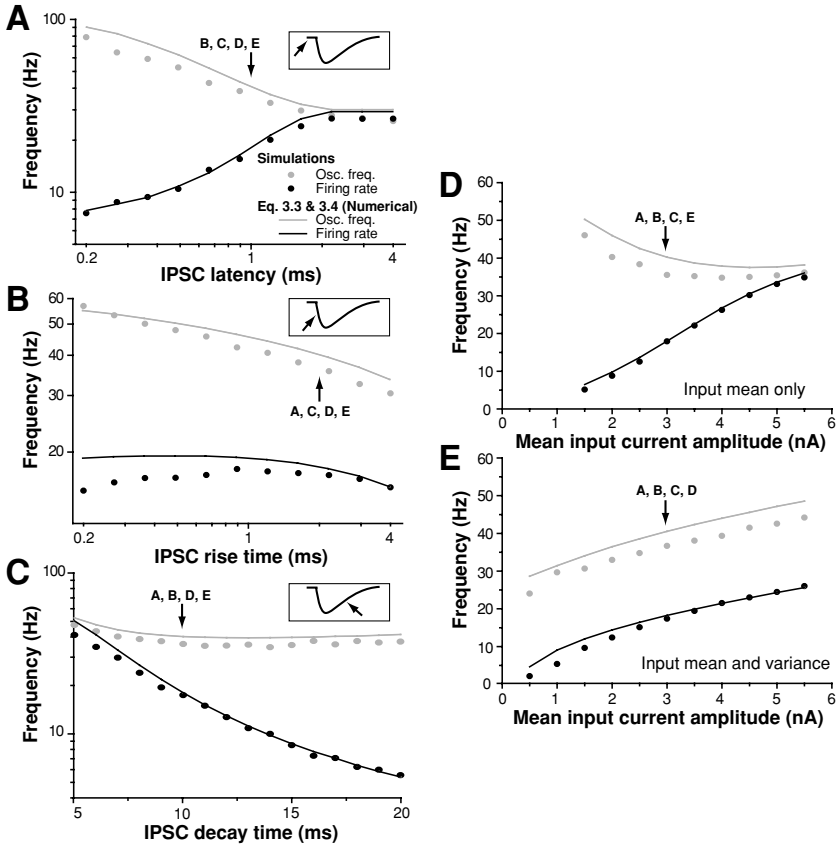

Figure 5: Influence of synaptic time constants and input parameters on firing rate and oscillation frequency for a gaussian distribution of inputs and conductance-based synapses. (A) Synaptic latency. (B) Rise time. (C) Decay time. (D) Input mean only. The standard deviation is fixed to $\sigma_I = 0.15$ nA. (E) Mean $\langle I \rangle$ and standard deviation σ_I of the input distribution are both changed in the same proportion and $\sigma_I = 0.05 \langle I \rangle$. Otherwise, if not varied, simulation parameters are: $M = 961$ neurons, $R = 100$ MΩ, $C = 500$ pF, $\theta = -52$ mV, $V_{\text{reset}} = VL = -70$ mV, $VG = -70$ mV, $\tau_d = 10$ ms, $\tau_r = 2$ ms, $\tau_l = 1$ ms, $\langle I \rangle = 3$ nA, $\sigma_I = 0.05 \langle I \rangle$, and the peak conductance of single inhibitory events $G_{\max} = 2$ nS.

$s(t)$ as in equation 2.3 with a decay time τ_d much larger than the rise time, the mean conductance is given by

$$\langle G \rangle_t = G_{\max} \frac{N \tau_d}{T}. \tag{5.1}$$

Because the membrane time constant now depends on the two unknown parameters N and T, the solution $r_{N,T}(t)$ of the spike time equation is also a function of N and T. However, both N and T can be determined by solving $N = \int r_{N,T}(t) e^{\frac{t}{\tau_d}} dt$ together with equation 3.3 for the oscillation period. This can be easily performed numerically, yielding predictions that are in good agreement with simulations of the full network (e.g., for a gaussian distribution of inputs in Figure 4B). The results interestingly show that the dependencies of oscillation frequency on inhibition strength (compare Figures 4A and 4B) and on synaptic time constants (compare Figures 3 and 5) are similar for current- and conductance-based synapses, indicating that conductance effects have little influence on the qualitative behavior of the oscillation. The intuitive explanation of this observation is that the quantity N/T is roughly equal to the time-averaged network firing rate, which for large J varies close to linearly with the inverse of $G_{\max}$ and τ_d and depends little on τ_r (see Figures 3, 4, and 5). Hence, $\langle G \rangle_t$ can have only a weak contribution on oscillation properties.

5.3 Extension to Partial Connectivity. It should be accounted for that in biological networks, each neuron is connected to only a fraction of the other neurons. In this case, the total current (or conductance) received in each cell i becomes a random variable. If we take the simple example of a randomly connected network with constant probability $p < 1$, then the number of synaptic events received by each neuron is roughly $Np(1 + \sigma_N \chi_i)$, where χ_i is a random variable with a unitary gaussian distribution (in the limit of large N) and with $\sigma_N = \sqrt{\frac{1-p}{pN}}$. This gives a slightly modified equation for the spike times:

$$0 = -U_k + J\,pNA_d \frac{(1 + \sigma_N \chi_k) e^{-\frac{T + t_k - \tau_l}{\tau_d}}}{1 - e^{-\frac{T}{\tau_d}}} + J\,p \sum_{l=0}^{k-1} v_{\text{single}}(t_k - t_l). \tag{5.2}$$

The period T is defined by

$$\frac{U_{i_0}}{1 + \sigma_N \chi_{i_0}} = \frac{J\,pNA_d e^{-\frac{T - \tau_l}{\tau_d}}}{1 - e^{-\frac{T}{\tau_d}}}, \tag{5.3}$$

in which i_0 stands for the index of the first neuron that is able to reach the threshold at the end of the silent phase. Setting $Z_0 = \frac{U_{i_0}}{1 + \sigma_N \chi_{i_0}}$, equation 5.2 can

be simplified into the same form as equation 3.4 if we neglect the quantity $Z_0\sigma_N\chi_k(1-\mathrm{e}^{-\frac{t}{\tau_d}})$:

$$0 = \tilde{U}_k + Z_0\mathrm{e}^{-\frac{t'_k}{\tau_d}} + J\,p\sum_{l=0}^{k-1} v_{\text{single}}(t'_k - t'_l). \tag{5.4}$$

In this form, the effective heterogeneity in the network $\tilde{U}_k = U_k - Z_0\sigma_N\chi_i$ is simply the sum of input and synaptic heterogeneities. If we consider the case in which the U_k's are normally distributed with variance σ_U^2, $\tilde{U}_k$ also has a gaussian distribution with variance $\tilde{\sigma}_U^2 = \sigma_U^2 + Z_0^2\sigma_N^2$.

With this evaluation of the effective variance of heterogeneities, we can obtain good agreement between the numerical solution of the spike time equation and simulations of the full network. Interestingly we observe that the frequency of oscillation goes through a minimum for large inhibition strengths (see Figure 4C). This is due to synaptic heterogeneities that dominate over input heterogeneities in the limit of strong inhibition. The variance of the total synaptic current received by a neuron is roughly linear in the strength of inhibition J ($\sigma_N^2 \sim N^{-1} \sim J$). This adds up with the tail effect of the gaussian distribution, increasing the effective voltage dispersion (i.e., effective ΔU) such that it can balance the increase in J, implying a stabilization of oscillation frequency (frequency depends on inhibition via the ratio of J over voltage dispersion; see section 4). A minimum in oscillation frequency for strong inhibition has already been reported in some numerical studies that consider networks of detailed neurons with biologically realistic inhibitory connectivity (Bathellier et al., 2006; Vida et al., 2006). We could verify that for the detailed neuron model used by Bathellier et al. (2006), partial connectivity is required to observe the minimum in oscillation frequency and therefore also explains this effect (see Figure 4D).

6 Link Between Fixed Heterogeneities and Temporal Noise

Our approach assumes fixed heterogeneous input currents and no noise. However convenient this "quenched noise" hypothesis might be, it is undeniable that real neurons also receive randomly fluctuating inputs. Inhibition-dependent oscillations in homogeneous, noise-driven networks and in heterogeneous, deterministic networks show one clear difference. For the former, all individual neurons fire irregularly but with the same overall firing rate (see Figures 6B and D), whereas for the latter, one fraction of the cells regularly fires at oscillation frequency while the rest is silent (see Figures 6A and 6D). That said, neither of these two extreme cases actually represents the biological reality because both fast noise and steady heterogeneities exist in brain networks, although it is not clear in which proportion. Hence, one should expect that neuronal firing in a brain network is not fully stochastic (see Figure 6C) and that the distribution of firing

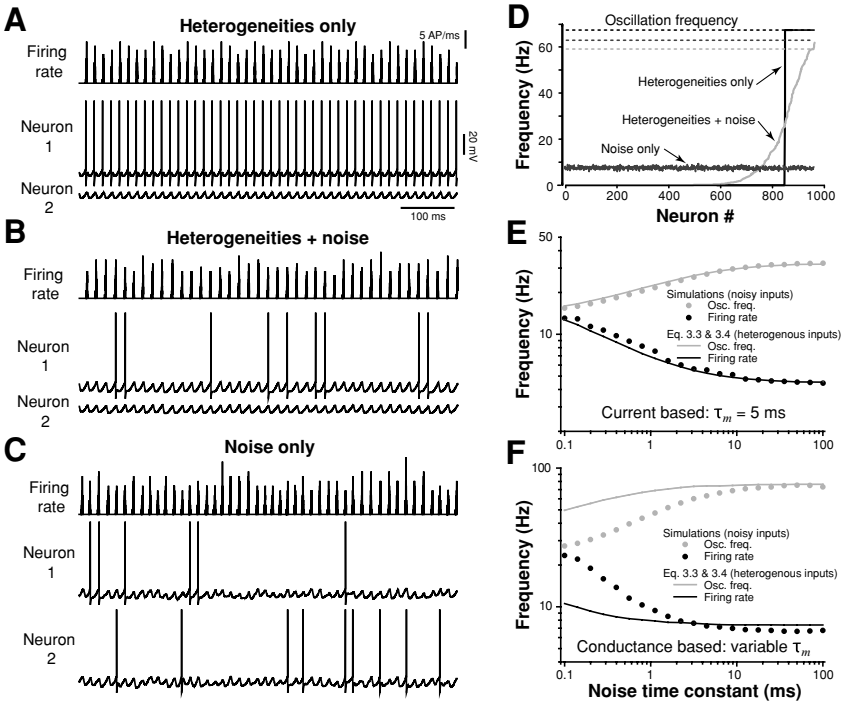

Figure 6: Link between heterogeneous and noisy inputs paradigms. (A–C) Instantaneous network firing rate and single neuron voltage traces for a network driven by heterogeneous steady inputs only (A), colored noise inputs only (C), or both (B). In *B*, noise and heterogeneities respectively contribute 30% and 70% of the total current standard deviation. Simulation parameters are as in Figure 4B with $G_{\max} = 2.6$ nS, $\tau_{\text{noise}} = 5$ ms. In A, $\sigma_I = 0.45$ nA. In *C*, $\sigma_{\text{noise}} = 0.45$ nA. In *B*, $\sigma_I = 0.315$ nA and $\sigma_{\text{noise}} = 0.135$ nA. (D) Distribution of neuronal firing rates for all 961 neurons of the network for the three mentioned cases. In the case of heterogeneity, neurons with a small index receive the weakest drive. The dashed lines represent the oscillation frequencies. From top to bottom: heterogeneities, noise, both. (E) Firing rate and oscillation frequency in a network driven by colored noise when the noise time constant is changed. Synapses are modeled as currents, and the membrane time constant τ_m is set to 5 ms. In this case, the heterogeneous input paradigm gives good analytical predictions. Parameters are as in Figure 4A, with $J = 0.92$ mV, $R\sigma_{\text{noise}} = 1$ mV, and no heterogeneity (i.e. $\sigma_I = 0$). (F) Same as *E* but for synapses modeled as conductances. In this case, the time constant is variable but smaller than 1 ms. The quality of the prediction drops for lower noise time constants. Parameters are as in Figure 4B but with $G_{\max} = 2.6$ nS, $\sigma_{\text{noise}} = 0.45$ nA and $\sigma_I = 0$.

rates in the population is heterogeneous but to some extent homogeneized by noise (see Figure 6D). Nevertheless, the full regularity of neuronal firing is not a requirement for the validity of our approach.

Indeed, our framework requires simply the statistics of the voltage dispersion to be constant from one cycle to another and the distribution of membrane voltages in the population to be constant during the period of discharge (this is explicitly supposed in the derivation of the spike time equation). The first condition is fulfilled if input currents are stationary stochastic processes, and the second condition simply imposes that voltage fluctuations are slow enough. Namely, our framework should remain valid as long as the duration of the period discharge T' is much smaller than the correlation time τ_v of the noisy membrane voltage. Voltage fluctuations result from the filtering of current inputs by the membrane dynamics, implying that their correlation time will be close to the largest of membrane time constant τ_m and of the correlation time of the noisy input τ_{noise}. Therefore, the slow noise hypothesis holds in any case if the membrane time constant is itself much larger than the duration of the period of discharge, and otherwise if input fluctuations are slow enough.

If we take σ^2_{noise} to be the variance of the noisy input (gaussian noise), it is easy to deduce the effective standard deviation of voltage fluctuations:

$$\sigma_U = \frac{\sigma_{\text{noise}}}{\sqrt{1 + \tau_m/\tau_{\text{noise}}}}. \tag{6.1}$$

In the slow noise limit, σ_U can be directly used as the standard deviation of the input currents U_k in order to solve the spike time equation (see equation 3.4). The condition $\tau_m \gg T'$ can be typically obtained with current-based synapses that do not affect the membrane time constant, and in this case, both oscillation frequency and network firing rate can be accurately predicted by our framework for any correlation time of the noisy input (see Figure 6E; $\tau_m = 5$ ms, discharge period: $\sim$1 ms). In contrast, if the membrane time constant is small (e.g., with strong activations of conductance-based synapses), the predictions of our framework can be accurate only for large noise correlation times (see Figure 6E; $\tau_m < 1$ ms, discharge period: 1–2 ms). When the noise correlation time is small, our approach actually tends to overestimate oscillation frequency and underestimate the average network firing rate, which means that the strength of the suppression phenomenon is overestimated. Fast noise is expected to increase the rate of threshold crossings as compared to heterogeneous, noise-free trajectories with the same variance. This leads to a more intense and narrower discharge period than predicted and results in a prolongation of the oscillation period. It is noteworthy that in principle, this effect does not affect in their substance the mechanisms described in the noise-free case and that parameter dependencies should be qualitatively the same for fast noise as for heterogeneous networks. It is therefore not surprising that, for example, the dependencies

of oscillation frequency on the synaptic time constants in the heterogeneous case are qualitatively very similar to those already observed in the noisy case (compare Figures 3 and 5 with Geisler, Brunel, & Wang 2005; Brunel & Wang 2003). Conversely, our approach can be very useful for accurately predicting the behavior of oscillations in noisy networks with respect to variations of any parameter, in a strongly nonlinear regime where existing approaches are not adequate.

7 Discussion

We have presented an analytical framework in which it is possible to compute explicitly the instantaneous firing of a recurrent inhibitory network of spiking neurons in the regime of fully developed oscillations. This framework also assumes that only a fraction of the neurons fires in each oscillation cycle, which corresponds to the so-called suppressive or low-firing-rate regime, generally observed in the brain during in vivo and in vitro gamma-band oscillations. The particularity of this regime, as compared to the case where all neurons are able to fire on each cycle, is that the number of spikes per cycle is a priori unknown. We have show here a method to estimate this number as well as the time course of the network discharge in the cycle. Oscillation frequency and mean firing rate are deduced from this estimation.

Our computations are valid in a regime where the membrane time constant (τ_m) is clearly smaller than oscillation period (T) and inhibition decay time (τ_d). This so-called phasic regime has been identified by others as the only regime in which oscillations in deterministic inhibitory integrate-and-fire networks are stable with respect to input heterogeneities (Chow, 1998; White et al., 1998). As a consequence, suppression can occur only within the "phasic" regime. It is noteworthy that oscillation frequency in the phasic regime has been readily computed for homogeneous networks (i.e. no suppression; Chow et al., 1998). The result resembles our formula 4.7 in that it is the product of τ_d and of a logarithmic term. However, the argument of the logarithm clearly differs in the two formulas. The main specificities of the "suppressive" regime as opposed to the homogeneous "phasic" regime are the absence of dependency on mean input strength, the presence of dependencies in synaptic rise time and membrane time constant, and the square root dependency on synaptic strength (instead of linear).

Our framework applies to networks of neurons driven by steady heterogeneous currents or having slow-voltage fluctuations. "Slow" in this case means that the noise correlation time should be clearly larger than the duration T' of the discharge but can be shorter than the period T of the oscillation. On the basis of our current knowledge, it is difficult to decide if this condition holds for brain networks in general, in particular because noise has been very little studied experimentally in relation to oscillations. It can nevertheless be argued that most of the noisiness in the

membrane voltage of neurons is due to synaptic activity, which, according to the decay time of typical synaptic events, gives correlation times in the range of several milliseconds (about 2 to 10 ms depending on the type of synapse). A recent report also indicates that inhibition actually dominates membrane voltage fluctuations, which implies rather slow correlation times (about 10 ms; Rudolph, Pospischil, Timofeev, & Destexhe, 2007). Such a value would be close to the slow noise limit (e.g., in the hippocampus), but further research is needed to check this possibility. Finally, a high enough membrane time constant can also give slow voltage fluctuations, even if to the best of our knowledge, there are no clear experimental statements about the values of effective membrane time constants during gamma oscillations.

If noise is an important part of the natural inputs received by a neuron, it is also true that heterogeneities are plentiful in the brain. Real neurons (even belonging to the same class) have discrepancies in their size and shape, as well as in the distribution and density of their active channels, all of which can constitute nonnegligible heterogeneities. In addition, the natural input currents to brain networks are expected to be nonuniform, precisely because their distribution should contain some information. What remains unclear is to which proportion noise and heterogeneities contribute to the dispersion of membrane voltages in biological networks. In fact, as we suggested in Figures 6A to 6D, this proportion could be inferred from the regularity of individual neurons firing. If neurons tend either to fire at oscillation frequency or to be silent, as seems to be the case for odor-induced gamma oscillation in the olfactory bulb (Buonviso et al., 2003), then steady heterogeneities are dominant. If, on the contrary, neurons seem to fire sparsely and in very random fashion (like pyramidal cells in hippocampal slices; Hajos et al., 2004; Fisahn et al., 1998), then noise is more important.

Our analysis gives several predictions relative to the control of oscillation frequency and network firing rate by synaptic and input parameters. In particular, we demonstrate that the low-firing-rate regime implies a relative stability of oscillation frequency over large variations of inhibition amplitude, which contrasts with important changes of the network mean firing rate. This particular behavior was recently observed in olfactory bulb slices (Bathellier et al., 2006), suggesting that a single inhibitory loop between olfactory bulb principal neurons could be mediating gamma oscillations in this structure (see the discussion about the supposed synaptic mechanisms in the olfactory bulb made by Bathellier et al., 2006). In hippocampal slices, there exist at least two types of gamma oscillations. The first type (termed interneuron network gamma or ING by Whittington et al., 2000) involves only the interneurons' circuit and would correspond to our hypothesis of a single population of inhibitory neurons. In fact, no stability of oscillation frequency is observed for the ING oscillations, indicating in the light of our results that these oscillations should not have suppression. In contrast,

the second type of hippocampal gamma oscillation (generated by different induction protocols as the ING) exhibits a stability of oscillation frequency with respect to pharmacological modulation of inhibition strength (Fischer & Durr, 2003; Faulkner et al., 1998). It was demonstrated that for these protocols, the oscillation requires the interplay of excitatory and inhibitory neurons (this type of oscillation was termed PING—pyramidal-interneuron network gamma—by Whittington et al. 2000). Moreover, it is possible that at least two inhibitory loops are involved in the generation of these hippocampal gamma rhythms. Indeed, experimental analysis of postsynaptic currents suggests that excitatory inputs from pyramidal cells drive interneuron populations, which in turn release inhibition in pyramidal neurons (Oren, Mann, Paulsen, & Hajos, 2006). Along with this first loop, direct recurrent inhibition between interneurons is also observed to play a nonnegligible role (Oren et al., 2006). This represents a larger degree of complexity than was included in our simple model. Therefore, an extension of our framework to multiple loops would in fact be necessary to capture the mechanism of the PING oscillatory dynamics. Such an extension would consist in coupling the spike timing equations of each neural population. Although it would complicate the mathematical analysis, the case of multiple loops would not fundamentally change the formalism that we have presented here. Such an extension seems promising because our hypothesis of highly nonlinear, narrow spike time distribution appears to particularly well fit both interneurons and pyramidal cell data (Hajos et al., 2004) and because pyramidal neurons fires at a low rate (Fisahn et al., 1998). In this respect, it is noteworthy that the spike distribution of pyramidal neurons in the oscillatory cycle has a shape very similar to what we observe in our simple network for gaussian heterogeneities (a slow increase in spike probability followed by a steep decrease; see Figures 1 and 3 and compare with Hajos et al., 2004), indicating that a suppression phenomenon similar to what we modeled in this study might participate in the PING hippocampal oscillations.

On a more conceptual but still practical level, one important point that we want to make with this study is about the phenomenon of suppression (White et al., 1998; Chow et al., 1998). The role of suppression on oscillation properties in a heterogeneous network is not taken into account in many experimental and theoretical studies, probably because it is not fully intuitive. Moreover, if the presence of suppression is easy to acknowledge when neuronal firing is slow and irregular, it is less obvious when most neurons fire in a regular fashion and others are silent. The latter regime can thus falsely be confused with a pure synchronized oscillator regime. However, these regimes are somewhat different. Suppression gives, for example, much more flexibility for adjusting the rate of the population output while maintaining a stable oscillation frequency. It also represents a mechanism that selects which neurons are allowed to fire and forces them into synchronous firing. So if suppression is taking place, gamma oscillations are the correlate

not only of the establishment of synchrony but also of a competitive mechanism. We therefore think that it is crucial to study suppression as such in the context of gamma rhythms, for both better mechanistic understanding of the phenomenon and capturing the role of fast oscillations in the treatment and propagation of information in the brain.

Appendix A: Derivation of the Instantaneous Firing Rate Equation

We here give the main steps for obtaining equation 4.3. We start from equation 4.2, which can be rewritten as

$$r(t) + \frac{J\,M}{\Delta U}\frac{\mathrm{d}}{\mathrm{d}t}\int_0^t r(x)v_{\mathrm{single}}(t-x)\,dx = \frac{MU_{i_0}}{\tau_d\,\Delta U}\mathrm{e}^{-\frac{t}{\tau_d}}, \tag{A.1}$$

with

$$v_{\mathrm{single}}(t) = \int_0^t s(y)\mathrm{e}^{-\frac{t-y}{\tau_m}}dy, \tag{A.2}$$

where $s(y) = \mathrm{e}^{-\frac{y}{\tau_d}} - \mathrm{e}^{-\frac{y}{\tau_r}}$ is the time course of a unitary synaptic current. At $t = 0$, the time derivative of the integral term in equation A.1 is equal to $r(0)v_{\mathrm{single}}(0) = 0$, giving the initial condition $r(0) = \frac{MU_{i_0}}{\tau_d\,\Delta U}$. We then make the assumption that $\mathrm{e}^{-\frac{t}{\tau_d}} \simeq 1$ (i.e., zero-order approximation in T/τ_d), such that the derivative of the synaptic current waveform can be approximated by $\mathrm{e}^{-\frac{y}{\tau_r}}/\tau_r$ and the right-hand side of equation A.1 is constant. Hence, after deconvolution of equation A.1 by the differential operator $(\tau_m\frac{\mathrm{d}}{\mathrm{d}t}\cdot + \cdot)$, we obtain

$$\tau_m\frac{\mathrm{d}r}{\mathrm{d}t} + r(t) + \frac{J\,M}{\Delta U\tau_r}\int_0^t r(x)\mathrm{e}^{-\frac{t-x}{\tau_r}}\,dx = \frac{MU_{i_0}}{\tau_d\,\Delta U}. \tag{A.3}$$

The integral term being null at $t = 0$, it is straightforward to derive from this equation the second initial condition: $\frac{\mathrm{d}r}{\mathrm{d}t}(0) = 0$. Finally, application of the operator $(\tau_r\frac{\mathrm{d}}{\mathrm{d}t}\cdot + \cdot)$ to equation A.3 yields the second-order differential equation for $r(t)$:

$$\tau_m\tau_r\frac{\mathrm{d}^2r}{\mathrm{d}t^2} + (\tau_m + \tau_r)\frac{\mathrm{d}r}{\mathrm{d}t} + \left(1 + \frac{J\,M}{\Delta U}\right)r(t) = \frac{MU_{i_0}}{\tau_d\,\Delta U}. \tag{A.4}$$

Appendix B: Reduction of the Neuron Model for Conductance-Based Synapses

For neurons receiving conductance-based synaptic inputs, the voltage equation reads:

$$C\frac{\mathrm{d}V_i}{\mathrm{d}t} = -\frac{1}{R}(V_i - V_L) + I_i^{het} - G_i(t)(V_i - E_{syn}), \tag{B.1}$$

where E_{syn} is the reversal potential of inhibitory synapses. We rewrite the synaptic term as a function of the new membrane voltage variable $v_i = V_i - \theta$ and of the time average of the total conductance $\langle G_i \rangle_t$:

$$G_i(t)(V_i - E_{syn}) = G_i(t)(\theta - E_{syn}) + \langle G_i \rangle_t v_i + v_i(G_i(t) - \langle G_i \rangle_t). \tag{B.2}$$

Supposing that $G(t)$ varies little around its time average and that v_i stays close to 0, we can neglect the product $v_i(G_i(t) - \langle G_i \rangle_t)$ in this expression. In this case, the voltage can be described by the same canonical equation as for the current-based model:

$$v_i(t) = U_i^* + (V_{reset} - \theta - U_i^*)\mathrm{e}^{-\frac{t-\hat{t}_i}{\tau_m^*}} - \frac{1}{\tau_m^*}\int_{\hat{t}_i}^{t} \mathrm{e}^{-\frac{t-x}{\tau_m^*}} \alpha_i^*(x)\,dx, \tag{B.3}$$

with $\tau_m^* = R^*C$, $R^* = \frac{R}{1+R\langle G_i \rangle_t}$, $U_i^* = (V_L - \theta)R^*/R + R^* I_i^{het}$ and the effective synaptic current $\alpha_i^*(t) = R^*(\theta - E_{syn})G_i(t)$.

References

Abbott, L. F., & van Vreeswijk, C. (1993). Asynchronous states in networks of pulse-coupled oscillators. *Physical Review E, 48*(2), 1483–1490.

Adrian, E. D. (1942). Olfactory reactions in the brain of the hedgehog. *J. Physiol., 100*(4), 459–473.

Bartos, M., Vida, I., Frotscher, M., Meyer, A., Monyer, H., Geiger, J. R., & Jonas, P. (2002). Fast synaptic inhibition promotes synchronized gamma oscillations in hippocampal interneuron networks. *Proc. Natl. Acad. Sci. USA, 99*(20), 13222–13227.

Bartos, M., Vida, I., & Jonas, P. (2007). Synaptic mechanisms of synchronized gamma oscillations in inhibitory interneuron networks. *Nat. Rev. Neurosci., 8*(1), 45–56.

Bathellier, B., Lagier, S., Faure, P., & Lledo, P.-M. (2006). Circuit properties generating gamma oscillations in a network model of the olfactory bulb. *J. Neurophysiol., 95*(4), 2678–2691.

Brunel, N. (2000). Dynamics of sparsely connected networks of excitatory and inhibitory spiking neurons. *J. Comput. Neurosci., 8*(3), 183–208.

Brunel, N., & Hakim, V. (1999). Fast global oscillations in networks of integrate-and-fire neurons with low firing rates. *Neural. Comput., 11*(7), 1621–1671.

Brunel, N., & Wang, X.-J. (2003). What determines the frequency of fast network oscillations with irregular neural discharges? I. Synaptic dynamics and excitation-inhibition balance. *J. Neurophysiol., 90*(1), 415–430.

Buhl, E. H., Tamas, G., & Fisahn, A. (1998). Cholinergic activation and tonic excitation induce persistent gamma oscillations in mouse somatosensory cortex in vitro. *J. Physiol., 513 (Pt 1)*, 117–126.

Buonviso, N., Amat, C., Litaudon, P., Roux, S., Royet, J.-P., Farget, V., et al. (2003). Rhythm sequence through the olfactory bulb layers during the time window of a respiratory cycle. *Eur. J. Neurosci., 17*(9), 1811–1819.

Chow, C. C. (1998). Phase locking in weakly heterogeneous networks. *Physica D, 118*, 343–370.

Chow, C. C., White, J. A., Ritt, J., & Kopell, N. (1998). Frequency control in synchronized networks of inhibitory neurons. *J. Comput. Neurosci., 5*(4), 407–420.

Csicsvari, J., Hirase, H., Czurko, A., & Buzsaki, G. (1998). Reliability and state dependence of pyramidal cell–interneuron synapses in the hippocampus: An ensemble approach in the behaving rat. *Neuron, 21*(1), 179–189.

Davison, A. P., Feng, J., & Brown, D. (2003). Dendrodendritic inhibition and simulated odor responses in a detailed olfactory bulb network model. *J. Neurophysiol., 90*(3), 1921–1935.

Destexhe, A., Rudolph, M., & Pare, D. (2003). The high-conductance state of neocortical neurons in vivo. *Nat. Rev. Neurosci., 4*(9), 739–751.

Faulkner, H. J., Traub, R. D., & Whittington, M. A. (1998). Disruption of synchronous gamma oscillations in the rat hippocampal slice: A common mechanism of anaesthetic drug action. *Br. J. Pharmacol., 125*(3), 483–492.

Fisahn, A., Pike, F. G., Buhl, E. H., & Paulsen, O. (1998). Cholinergic induction of network oscillations at 40 Hz in the hippocampus in vitro. *Nature, 394*(6689), 186–189.

Fischer, Y., & Durr, R. (2003). Inhibitory control of intrinsic hippocampal oscillations? *Brain Res., 982*(1), 79–91.

Freeman, W. J. (1972). Measurement of oscillatory responses to electrical stimulation in olfactory bulb of cat. *J. Neurophysiol., 35*(6), 762–779.

Freeman, W. J. (1975). *Mass action in the nervous system*. New York: Academic Press.

Friedrich, R. W., Habermann, C. J., & Laurent, G. (2004). Multiplexing using synchrony in the zebrafish olfactory bulb. *Nat. Neurosci., 7*(8), 862–871.

Geisler, C., Brunel, N., & Wang, X.-J. (2005). Contributions of intrinsic membrane dynamics to fast network oscillations with irregular neuronal discharges. *J. Neurophysiol., 94*(6), 4344–4361.

Gerstner, W. (2000). Population dynamics of spiking neurons: Fast transients, asynchronous states, and locking. *Neural Comput., 12*(1), 43–89.

Gerstner, W., & van Hemmen, J. L. (1993). Coherence and incoherence in a globally coupled ensemble of pulse-emitting units. *Phys. Rev. Lett., 71*(3), 312–315.

Gerstner, W., Ritz, R., & van Hemmen, J. L. (1993). A biologically motivated and analytically soluble model of collective oscillations in the cortex. *Biol. Cybern., 68*, 363–374.

Gerstner, W., van Hemmen, J. L., & Cowan, J. D. (1996). What matters in neuronal locking? *Neural Comput., 8*(8), 1653–1676.

Gray, C. M., & Singer, W. (1989). Stimulus-specific neuronal oscillations in orientation columns of cat visual cortex. *Proc. Natl. Acad. Sci. USA, 86*(5), 1698–1702.

Hajos, N., Palhalmi, J., Mann, E. O., Nemeth, B., Paulsen, O., & Freund, T. F. (2004). Spike timing of distinct types of GABAergic interneuron during hippocampal gamma oscillations in vitro. *J. Neurosci., 24*(41), 9127–9137.

Hansel, D., & Mato, G. (2003). Asynchronous states and the emergence of synchrony in large networks of interacting excitatory and inhibitory neurons. *Neural Comput., 15*(1), 1–56.

Kaiser, J., & Lutzenberger, W. (2003). Induced gamma-band activity and human brain function. *Neuroscientist, 9*(6), 475–484.

Kopell, N., & Ermentrout, B. (2004). Chemical and electrical synapses perform complementary roles in the synchronization of interneuronal networks. *Proc. Natl. Acad. Sci. USA, 101*(43), 15482–15487.

Lagier, S., Carleton, A., & Lledo, P.-M. (2004). Interplay between local GABAergic interneurons and relay neurons generates gamma oscillations in the rat olfactory bulb. *J. Neurosci., 24*(18), 4382–4392.

Lagier, S., Panzanelli, P., Russo, R. E., Nissant, A., Bathellier, B., Sassoe-Pognetto, M., et al. (2007). GABAergic inhibition at dendrodendritic synapses tunes gamma oscillations in the olfactory bulb. *Proc. Natl. Acad. Sci. USA, 104*(17), 7259–7264.

Neltner, L., Hansel, D., Mato, G., & Meunier, C. (2000). Synchrony in heterogeneous networks of spiking neurons. *Neural Comput., 12*(7), 1607–1641.

Oren, I., Mann, E. O., Paulsen, O., & Hajos, N. (2006). Synaptic currents in anatomically identified CA3 neurons during hippocampal gamma oscillations in vitro. *J. Neurosci., 26*(39), 9923–9934.

Rudolph, M., Pospischil, M., Timofeev, I., & Destexhe, A. (2007). Inhibition determines membrane potential dynamics and controls action potential generation in awake and sleeping cat cortex. *J. Neurosci., 27*(20), 5280–5290.

Schoffelen, J.-M., Oostenveld, R., & Fries, P. (2005). Neuronal coherence as a mechanism of effective corticospinal interaction. *Science, 308*(5718), 111–113.

Sejnowski, T. J., & Paulsen, O. (2006). Network oscillations: Emerging computational principles. *J. Neurosci., 26*(6), 1673–1676.

Singer, W., & Gray, C. M. (1995). Visual feature integration and the temporal correlation hypothesis. *Annu. Rev. Neurosci., 18*, 555–586.

Strogatz, S. H., & Mirollo, R. E. (1991). Asynchronous states in networks of pulse-coupled oscillators. *J. Stat. Phys., 63*, 613–635.

Traub, R. D., Bibbig, A., LeBeau, F. E. N., Buhl, E. H., & Whittington, M. A. (2004). Cellular mechanisms of neuronal population oscillations in the hippocampus in vitro. *Annu. Rev. Neurosci., 27*, 247–278.

Traub, R. D., Whittington, M. A., Stanford, I. M., & Jefferys, J. G. (1996). A mechanism for generation of long-range synchronous fast oscillations in the cortex. *Nature, 383*(6601), 621–624.

van Vreeswijk, C., Abbott, L. F., & Ermentrout, G. B. (1994). When inhibition not excitation synchronizes neural firing. *J. Comput. Neurosci., 1*(4), 313–321.

Varela, F., Lachaux, J. P., Rodriguez, E., & Martinerie, J. (2001). The brainweb: Phase synchronization and large-scale integration. *Nat. Rev. Neurosci., 2*(4), 229–239.

Vida, I., Bartos, M., & Jonas, P. (2006). Shunting inhibition improves robustness of gamma oscillations in hippocampal interneuron networks by homogenizing firing rates. *Neuron, 49*(1), 107–117.

Wang, X. J., & Buzsáki, G. (1996). Gamma oscillation by synaptic inhibition in a hippocampal interneuronal network model. *J. Neurosci., 16*, 6402–6413.

Wehr, M., & Laurent, G. (1996). Odour encoding by temporal sequences of firing in oscillating neural assemblies. *Nature, 384*(6605), 162–166.

White, J. A., Chow, C. C., Ritt, J., Soto-Trevio, C., & Kopell, N. (1998). Synchronization and oscillatory dynamics in heterogeneous, mutually inhibited neurons. *J. Comput. Neurosci., 5*(1), 5–16.

Whittington, M. A., Traub, R. D., Kopell, N., Ermentrout, B., & Buhl, E. H. (2000). Inhibition-based rhythms: Experimental and mathematical observations on network dynamics. *Int. J. Psychophysiology, 38*, 315–336.

Received October 23, 2007; accepted March 5, 2008.